IEEE Access
Multidisciplinary | Rapid Review | Open Access Journal

Received 14 April 2023, accepted 22 April 2023, date of publication 25 April 2023, date of current version 3 May 2023.

Digital Object Identifier 10.1109/ACCESS.2023.3270262

RESEARCH ARTICLE

Comparative Analysis of Three-Phase PV Grid Connected Inverter Current Control Schemes in Unbalanced Grid Conditions

NAGWA F. IBRAHIM[1], KARAR MAHMOUD[2,3], (Senior Member, IEEE), MATTI LEHTONEN[2], AND MOHAMED M. F. DARWISH[4], (Senior Member, IEEE)

[1]Electrical Department, Faculty of Technology and Education, Suez University, Suez 43527, Egypt
[2]Department of Electrical Engineering and Automation, School of Electrical Engineering, Aalto University, 02150 Espoo, Finland
[3]Department of Electrical Engineering, Faculty of Engineering, Aswan University, Aswan 81542, Egypt
[4]Department of Electrical Engineering, Faculty of Engineering at Shoubra, Benha University, Cairo 11629, Egypt

Corresponding authors: Nagwa F. Ibrahim (nagwa.ibrahim@ind.suezuni.edu.eg), Karar Mahmoud (karar.mostafa@aalto.fi), and Mohamed M. F. Darwish (mohamed.darwish@feng.bu.edu.eg)

This work was supported by the Department of Electrical Engineering and Automation, Aalto University, Espoo, Finland.

ABSTRACT Recently, the regulation of photovoltaic inverters, effectively under imbalanced voltages on the grid, has been crucial for the operation of grid-connected solar systems. In this regard, determining the output current reference is an integral aspect of managing a solar inverter with an unbalanced voltage. Based on evaluations of Instantaneous Active-reactive Control (IARC), Positive Negative Sequence Control (PNSC), Balanced Positive Sequence Control (BPSC), and Average Active-reactive Control (AARC), this paper proposes a novel variable-current-t-reference calculation method for minimizing power fluctuations and current harmonics. The controller is employed to regulate both constructive and destructive sequences inside a static framework, therefore enhancing dynamic performance and facilitating the selection of suitable controls in the presence of significant network defects. This study also suggests comparing the four MPPT methodologies examined (fuzzy logic, current only, Incremental Conductance, and Perturb & Observe) to maximize energy output. The simulation results efficiently validate the suggested computation approach that is presented in the current reference.

INDEX TERMS Grid-connected PV system, output current reference, dual controller, current harmonics, MPPT techniques, and DC-DC converter.

I. INTRODUCTION

Power ripple and current harmonics at the photovoltaic (PV) inverter's output are amplified in the presence of negative sequence voltage due to the grid's instabilities. Among the most difficult parts of controlling PV inverters are the computations of the current reference and current control structure [1], [2]. PV inverter current reference may be calculated using several different methods, each of which is optimized for a specific goal, such as instantaneous real and reactive power regulation.

To minimize active, reactive, and negative sequence current, three types of output current reference algorithms were developed in [3], and [4]. However, none of them can eliminate reactive, active power fluctuations, and negative sequence currents simultaneously. Instantaneous active-reactive control (IARC), average active-reactive control (AARC), and balanced positive control (BPC) all describe different types of reactive controls. In [5], and [6], a method called flexible management of the negative and positive sequences (FPNSC) was created. FPNSC uses two parameters to manage oppositely charged sequence currents with greater flexibility; however, the method is complex and results in power fluctuations. Although PNSC-based advancements were made in [7], this approach can still not simultaneously eliminate active and reactive power fluctuations.

The associate editor coordinating the review of this manuscript and approving it for publication was Giambattista Gruosso.

Using a SIC-based three-phase inverter prototype, the suggested control is evaluated experimentally under a variety of network imbalance scenarios [8]. In addition, a reinforcement learning-based method for efficient transmission of PV transformers in unbalanced distribution networks the results [9] show that the proposed method converges with the optimal solution or with solutions with a surplus of PV energy reduction of less than 2.5 percent over many implementations while maintaining strict control of the amount of voltage. This research presents a time-domain symmetrical component extraction technique to separate the three-phase system into positive, negative, and zero sequences. As a result, a PI controller regulates the currents of the symmetric components. Also, a current auto-disturbance-rejection controller is developed, which, under unbalanced situations, decreases the grid-side current's harmonic content and speeds up the system's tracking reaction time. To obtain the quality of the grid-side current waveform, we added a notch filter to the modulation link, and the phase-locked loop structure is altered to reduce the impact of the third low-frequency harmonic component [10], [11].

A novel commonly grounded flying inductor-based converter has been presented in [12] as more than just a power electronic devices interface that can implement towards both single-phase ac and dc grids while utilizing the same connections. The proposed methodology uses this architecture to permit a direct connection between both the converter's output's negative polarity and the negative terminal of its input dc source. The study of [13] introduces a brand-new grid inverter without a transformer which includes six power electronic switches and two power diodes that may create a seven-level output voltage waveform using the suggested configuration. The proposed design can also reduce photovoltaic systems' leakage current amplitudes, which is a key issue for grid-connected PV applications.

In this work, a three-phase CSI continuous control setting controller design control (CCS-MPC) for an imbalanced network is offered. The proposed technique uses grid voltage and a power reference as inputs to establish the current reference. The capacitor voltage plus and inductor current were both factored into the cost function to dampen the filter's oscillation. The required current vector can be obtained via SVPWM by locating the minimum of the cost function. The suggested technique permits fast CSI response with no oscillation in both balanced and unbalanced grids [14]. In [15], a module power balance control system is described to maintain uniform transmission power across all modules. In [16], and [17] seamless integration with PVPP may be established by optimizing design, operation, and control methods to produce higher PQ and green energy.

The harmonic distortions may be reduced to 2.77 percent, the reactive power is properly compensated with a power factor that is nearly unity, and dynamic performances are enhanced with a quick transient response [18]. Direct power control is used to improve the quality of the energy provided by the solar field [19], [20], [21]. A second-order voltage ripple reduction method is proposed for applications using unbalanced ac voltage [22], [23]. To mitigate power fluctuations and current harmonics, [24], [25] developed a flexible approach to computing the reference current by leveraging a variable. The proportional-resonant controller regulates the oppositely charged sequence in the fixed frame concurrently to improve the dynamic performance. A performance evaluation of the various reference current generation techniques helps choose the optimum control for reducing the harmonics of power oscillation [26], [27].

Power converters are used in distributed generation systems to interface with distribution lines, but unbalanced grid faults can affect them. To control active and reactive power during these faults, a new flexible power control strategy based on a reference current generator is proposed. The strategy includes current limitation control and maximizes active power transfer while minimizing reactive power transfer. The proposed strategy is investigated through simulations and uses a fractional order proportional integral controller to minimize steady-state error. The performance of the proposed controller has been compared to a multiple complex-coefficients filter-based controller and is found to be effective. The study's contribution is the use of a dual average filter-based phase-locked loop to separate PNS voltage and current components [28]. The proposed strategy aims to maximize the power delivery capability of the grid-connected inverter and fulfill requirements under unbalanced grid faults. The strategy achieves power flow and power sharing among distributed generation units, the utility grid, and load demand through a power management system. The strategy minimizes active-reactive power oscillations with flexible control parameters and includes an improved positive and negative sequence extractor for separating sequence components [29].

Many of the studies focus on explaining and analyzing how voltage imbalance on the network affects and controls voltages and currents, as well as any filters that may be present. But most of the studies also focused on compensating the voltage on the network during transient times through different technologies. The paper aims to reach an optimized solution for the power oscillation problem. To do so, four optimization methods are used for calculating current references and applied to them. Controlling the active and reactive power in a photovoltaic (PV) grid-connected system under unbalanced voltage conditions is essential for maintaining system stability and ensuring efficient power transfer. Several methods can be employed to achieve control of the active and reactive power in a PV system under unbalanced voltage, including the use of advanced control algorithms and devices such as flexible management of the negative and positive sequences (FPNSC), Instantaneous active-reactive control (IARC), average active-reactive control (AARC), and positive-negative sequence control (PNSC), but in this study, we used balanced positive control (BPC) with compared by

other methods where this method more activation and good control by comparing the other method.

Advanced control algorithms, such as the vector control algorithm, can be used to regulate the active and reactive power flow in the system, considering the unbalanced voltage conditions. The vector control algorithm adjusts the output of the PV system based on the measured voltage and current values to ensure that the active and reactive power flows are balanced and that the system remains stable. Power factor correction can also be used to control the active and reactive power in a PV system under unbalanced voltage conditions. By adjusting the phase angle between the voltage and current in the system, power factor correction can ensure that the active power flows are balanced and that the reactive power flows are minimized, leading to a more efficient transfer of power.

Reactive power compensation is another method that can be used to control the reactive power in a PV system under unbalanced voltage conditions. Reactive power compensation involves adjusting the reactive power output of the system to match the reactive power demand of the electrical grid. This can be achieved using capacitors or inductors that are connected in parallel or series with the PV system. In addition to these methods, devices such as voltage regulators and reactive power compensators can be used to control the active and reactive power flow in a PV system under unbalanced voltage conditions. Voltage regulators adjust the voltage output of the PV system to match the demand from the electrical grid, while reactive power compensators adjust the reactive power output to match the reactive power demand of the electrical grid.

In conclusion, controlling the active and reactive power in a PV grid-connected system under unbalanced voltage conditions is critical to maintaining system stability and ensuring efficient power transfer. Advanced control algorithms, power factor correction, reactive power compensation, voltage regulators, and reactive power compensators are some of the methods and devices that can be used to achieve this control. The selection of the appropriate control method depends on the specific characteristics of the PV system and the electrical grid.

The design approach in this paper aims to evaluate and compare four techniques (IARC, AARC, BPSC, and PNSC), for selecting the proposed method to minimize the power fluctuations and output current harmonics. This paper is organized as follows: Section II presents the PV inverter topology and mathematical models. Referencing current calculation methods is given in Section III which also introduces mathematically different methods for power control under fault duration and its bi-objective function. In addition, the control structure of the PV inverter. Active and reactive power controllers are explained in Section IV-A. Moreover, a dc voltage controller is proposed in Section IV-B. Further, Section IV-C discusses the outer controller of the system. Section V discusses various types of MPPT techniques, such as fuzzy logic control (FLC), current-only control (COC), Incremental Conductance (INC), and Perturb & Observe (P&O) methods. Simulation and comparative results are discussed to illustrate the proposed method's effectiveness in Section VI, and conclusions are presented in Section VII.

The contributions of this paper are summarized in the following points:

- For grid-connected PV systems to autonomously manage the active and reactive electricity supplied to the network under imbalanced operating situations, this study has given and analyzed four ways for producing current references. Simulation is employed to validate the theories and approximations used in the theoretical analysis of the techniques. Although the development of high-quality currents entails substantial power oscillations, the reduction of power fluctuations results in warped currents. It demonstrates how this kind of methodology is contingent mostly on the requirements of the power grid.
- This paper indicates comparing the INC-MPPT algorithm with a fuzzy logic controller, current only, and P&O for regulating the MPPT control of grid-connected PV systems. This fuzzy logic algorithm will allow the control signal and, consequently, the DC-DC converter's duty cycle to update to track the MPP with changes in the environmental conditions. The proposed FLC algorithm in this paper is compared to the other three control methods: P&O, INC, and current only with fuzzy controller algorithms. The FLC algorithm proved high performance and faster dynamic response for MPPT rather than other algorithms in some control indices, including overshoot, rise time, and settling time.
- This study adds to the current research on the impact of unbalanced grid conditions on PV system performance, which has received less attention compared to balanced grid conditions. The study identifies negative impacts such as reduced power output and increased voltage fluctuations and highlights the need for more investigation into renewable energy systems' performance under varying grid conditions. The findings can inform more efficient and reliable design and operation of PV systems in unbalanced grid regions.
- Additionally, the study examines the effects of unbalanced grid conditions on the DC-link and overcurrent resulting from the voltage imbalance.

II. PHOTOVOLTAIC INVERTER TOPOLOGY AND MATHEMATICAL DESIGN

Some of the features of the inverter and PV system shown in Figure 1 are the regulation of the DC voltage and the almost sinusoidal shape of the output current. A PV inverter's mathematical model looked like this [30], [31]:

$$V_{abc} = RI_{abc} + L\frac{dI_{abc}}{dt} + U_{abc} \tag{1}$$

where V_{abc} means the PV inverter's output voltage, I_{abc} represents the PV inverter's output current, and U_{abc} indicates

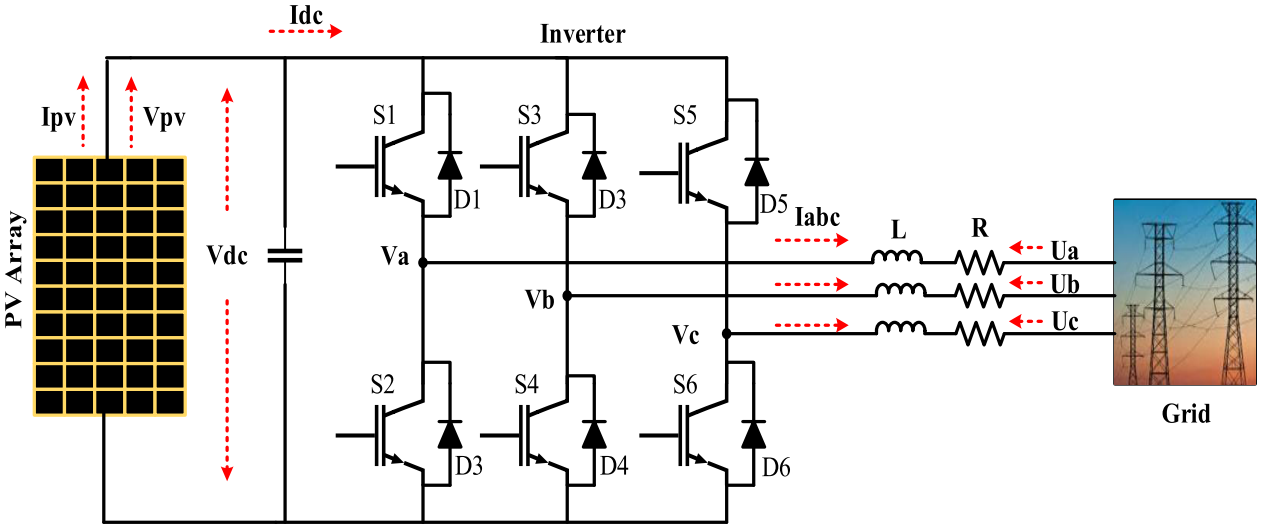

FIGURE 1. PV inverter structure.

the grid voltage. As a result, using the $\alpha\beta$ reference frame, the following mathematical model describes the operation of a PV inverter:

$$\left\{\begin{array}{l} V_\alpha = RI_\alpha + L\dfrac{dI_\alpha}{dt} + U_\alpha \\ V_\beta = RI_\beta + L\dfrac{dI_\beta}{dt} + U_\beta \end{array}\right\} \tag{2}$$

where Vα, Vβ denotes the output voltage components, Iα, Iβ denotes the output current components, and Uα, Uβ denotes the grid voltage components. On a DQ reference frame, the mathematical model of a PV inverter may be stated as follows:

$$\left\{\begin{array}{l} V_d^+ = (R+sL)\, I_d^+ - \omega L I_q^+ + U_d^+ \\ V_q^+ = (R+sL)\, I_q^+ - \omega L I_d^+ + U_q^+ \\ V_d^- = (R+sL)\, I_d^- - \omega L I_q^- + U_d^- \\ V_q^- = (R+sL)\, I_q^- - \omega L I_d^- + U_q^- \end{array}\right\} \tag{3}$$

where Vd +, Vq +, Vd−, and Vq− are the output voltage's DQ components symbolically. Id+, Iq+, Id−, and Iq− are outputs current's DQ components symbolically. U_d^+, U_q^+, $U_d^{-\prime} U_q^-$ are grid voltage's DQ components. The PV inverter's output p and q are computed using the instantaneous power theory [32].

$$P = V * I, \quad Q = V_\perp * I \tag{4}$$

at which V is the PV inverter's output voltage, I is a vector representing output current, and V⊥ is a 90° led V. The equations of V and V⊥ are written as:

$$\begin{aligned} \mathrm{V} &= (\mathrm{V_a}, \mathrm{V_b}, \mathrm{V_c})^{\mathrm{T}} \\ &= \begin{bmatrix} \mathrm{V}^+ \cos\left(\omega t + \varphi^+\right) + \mathrm{V}^- \cos\left(\omega t + \varphi^-\right) \\ \mathrm{V}^+ \cos\left(\omega \mathrm{t} - \dfrac{2}{3\pi} + \varphi^+\right) + \mathrm{V}^- \cos\left(\omega \mathrm{t} + \dfrac{2}{3\pi} + \varphi^-\right) \\ \mathrm{V}^+ \cos\left(\omega \mathrm{t} + \dfrac{2}{3\pi} + \varphi^+\right) + \mathrm{V}^- \cos\left(\omega \mathrm{t} - \dfrac{2}{3\pi} + \varphi^-\right) \end{bmatrix} \end{aligned} \tag{5}$$

$$\mathrm{V}_\perp = \frac{1}{\sqrt{3}} \begin{bmatrix} 0 & 1 & -1 \\ -1 & 0 & 1 \\ 1 & -1 & 0 \end{bmatrix} * V \tag{6}$$

where V+, V−, and φ+, φ− represent the amplitude and phase of the negative and positive sequence voltages, respectively.

A. PV MATHEMATICAL MODEL [33]

$$\begin{aligned} I &= I_{ph} - I_D \\ &= I_{ph} - I_O \left\{ exp\left[\frac{e\,(V + IRS)}{KTC}\right] - 1 \right\} \\ &\quad - \frac{V + IRS}{RSH} \end{aligned} \tag{7}$$

$$\begin{aligned} I &= I_{ph} - I_D \\ &= I_{ph} - I_O \left[exp\left[\frac{eV}{KTC}\right] - 1 \right] \end{aligned} \tag{8}$$

$$P_{max} = I_{max} * V_{max} \tag{9}$$

$$P_{max} = I_{sc} * V_{oc} * FF \tag{10}$$

$$FF = \frac{P_{max}}{I_{sc}} * V_{oc} = I_{max} * \frac{V_{max}}{I_{sc}} * V_{oc} \tag{11}$$

$$\exp\left(\frac{eV_{oc}}{KTC}\right) - 1 = \frac{I_{sc}}{I_o} \tag{12}$$

Which is solved for Voc:

$$V_{oc} = \frac{KTC}{e} \ln\left(\frac{I_{sc}}{I_o} + 1\right) = V_t \ln\left(\frac{I_{sc}}{I_o} + 1\right) \tag{13}$$

where another specified value for Vt thermal voltage (V) is

$$\mathrm{V_t} = \frac{\mathrm{KTC}}{\mathrm{e}} \tag{14}$$

The PV cell's generating power is determined by:

$$P = I * V \tag{15}$$

Suppose that V= I*R and that the power output is conditional upon this load resistance, R, and you get:

$$P = I^2 * R \tag{16}$$

Expression Eq. (7). into Eq. (16) provides:

$$P = \left\{ I_{sc} - I_o \left[\exp\left(\frac{eV}{KTC} \right) - 1 \right] \right\} V \tag{17}$$

Concerning V, equation (17) can be divided keeping the derivative's coefficient at 0.

$$\exp\left(\frac{\mathrm{eV_{max}}}{\mathrm{KTC}}\right)\left(1+\frac{\mathrm{eV_{max}}}{\mathrm{KTC}}\right) = 1+\frac{\mathrm{I_{sc}}}{\mathrm{I_o}} \tag{18}$$

$$\mathrm{I_{max}} = \mathrm{I_{sc}} - \mathrm{I_o}\left[\mathrm{e}^{\left(\frac{\mathrm{eV}}{\mathrm{KTC}}\right)} - 1\right] = \mathrm{I_{sc}} - \mathrm{I_o}\left[\frac{1+\frac{\mathrm{I_{sc}}}{\mathrm{I_o}}}{1+\frac{\mathrm{eV_{max}}}{\mathrm{KTC}}} - 1\right] \tag{19}$$

that also outcomes:

$$\mathrm{I_{max}} = \frac{\mathrm{eV_{max}}}{\mathrm{KTC}+\mathrm{eV_{max}}}(\mathrm{I_{sc}} + \mathrm{I_o}) \tag{20}$$

By using Eq. (5),

$$\mathrm{P_{max}} = \frac{\mathrm{eV^2{}_{max}}}{\mathrm{KTC}+\mathrm{eV_{max}}}(\mathrm{I_{sc}} + \mathrm{I_o}) \tag{21}$$

$$\eta_{\max} = \frac{\mathrm{P_{max}}}{\mathrm{P_{in}}} = \frac{\mathrm{I_{max}V_{max}}}{\mathrm{AG_t}} \tag{22}$$

III. DIFFERENT POWER CONTROL TECHNIQUES

A. ACTIVE REACTIVE CONTROL THAT IS IMMEDIATE (IARC)

States (3) that active power will just be provided through every current vector matched with both the voltage vector u, whereas reactive power would be created by any current vector connected with V⊥. The subsequent formulations, particularly form the cornerstone of the IARC methodology to detect the reference currents [32], [34], may be employed to describe this idea:

$$i_p = \frac{P}{|V|^2}V, \quad i_q = \frac{Q}{|V|^2}V_\perp \tag{23}$$

where $|V|^2$ seems to be the grid voltage vector's standard and has the following indicators:

$$|V|^2 = \left|V^+\right|^2 + \left|V^-\right|^2 + 2\left|V^+\right|\left|V^-\right|\cos\left(2\omega t + \varphi^+ - \varphi^-\right) \tag{24}$$

The final reference current of IARC strategy may be said to be:

$$i = i_p + i_q = \frac{PV + QV_\perp}{\left|V^+\right|^2 + 2V^+ * V^- + \left|V^-\right|^2} \tag{25}$$

Consequently, it is possible to compute the power output of a PV inverter using IARC as

$$p = V * i = V\left(\frac{P}{|V|^2} * V + \frac{Q}{|V|^2} * V_\perp\right) = P \tag{26}$$

$$\mathrm{q} = \mathrm{V}_\perp * \mathrm{i} = \mathrm{V}_\perp\left(\frac{\mathrm{P}}{|\mathrm{V}|^2} * V + \frac{\mathrm{Q}}{|\mathrm{V}|^2} * \mathrm{V}_\perp\right) = \mathrm{Q} \tag{27}$$

The reference power may be produced precisely by a PV inverter using the IARC technique, nevertheless, the reference current is not sinusoidal due to ripples in $|V|^2$ at 120 Hz.

$$i_p^* = g * v \tag{28}$$

$$i_q^* = b * v\perp \tag{29}$$

$$i_p^* * v = gv.v = P \Longrightarrow g\,|v|^2 = Pg = \frac{P}{|v|^2} \tag{30}$$

$$i_q^* * v\perp = bv\perp.v\perp = Q \Longrightarrow b\,|v|^2 \Longrightarrow b = \frac{Q}{|v|^2} \tag{31}$$

$$i_p^* = \frac{P}{|v|^2}v \tag{32}$$

$$i_q^* = \frac{Q}{|v|^2}v\perp \tag{33}$$

$$i^* = i_p^* + i_q^* \tag{34}$$

$$|v|^2 = v_a^2 + v_b^2 + v_c^2 = v_\alpha^2 + v_\beta^2 = v_d^2 + v_q^2 = m^2 \tag{35}$$

B. AVERAGE ACTIVE REACTIVE CONTROL (AARC)

The AARC technology utilizes VΣ^2 to compute the reference current rather than |V|^2 to eliminate the harmonics in the reference current acquired using the IARC strategy. VΣ^2 is determined as

$$\mathrm{V_\Sigma^2} = \left|\mathrm{V}^+\right|^2 + \left|\mathrm{V}^-\right|^2 \tag{36}$$

The reference current can thus be represented as

$$\mathrm{i} = \mathrm{i_p} + \mathrm{i_q} = \frac{\mathrm{PV} + \mathrm{QV}_\perp}{\left|\mathrm{V}^+\right|^2 + \left|\mathrm{V}^-\right|^2} \tag{37}$$

The PV inverter's output power may be computed as

$$p = P\left[1 + \frac{2\left|V^+\right|\left|V^-\right|}{\left|V^+\right|^2 + \left|V^-\right|^2}\cos\left(2\omega t + \phi^+ - \phi^-\right)\right] \tag{38}$$

$$q = Q\left[1 + \frac{2\left|V^+\right|\left|V^-\right|}{\left|V^+\right|^2 + \left|V^-\right|^2}\cos\left(2\omega t + \phi^+ - \phi^-\right)\right] \tag{39}$$

According to (36) and (37), the reference current is generally sinusoidal, nevertheless, there are 120-Hz fluctuations in the power output.

$$i_p^* = Gv; \quad G = \frac{P}{V_\Sigma^2} \tag{40}$$

$$i_q^* = Bv; \quad B = \frac{Q}{V_\Sigma^2} \tag{41}$$

$$V_\Sigma = \sqrt{\frac{1}{T}\int_0^T |U|^2\,dt} = \sqrt{\left|U^+\right|^2 + \left|U^-\right|^2} \tag{42}$$

$$p = i_p^*.u = \frac{|u|^2}{U_\Sigma^2}p = p + \check{p} \tag{43}$$

$$p = p\left[1 + \frac{2\left|v^+\right|\left|v^-\right|}{\left|v^+\right|^2 + \left|v^-\right|^2}\cos\left(2\omega t + \varphi^+ - \varphi^-\right)\right] \tag{44}$$

$$q = i_q^*.v\perp = \frac{|v|^2}{V_\Sigma^2}Q = Q \tag{45}$$

$$\mathrm{q} = \mathrm{Q}\left[1 + \frac{2\left|\mathrm{v}^+\right|\left|\mathrm{v}^-\right|}{\left|\mathrm{v}^+\right|^2 + \left|\mathrm{v}^-\right|^2}\cos\left(2\omega \mathrm{t} + \varphi^+ - \varphi^-\right)\right] \tag{46}$$

C. COMPENSATION FOR POSITIVE AND NEGATIVE SEQUENCES (PNSC)

Unbalanced currents are produced by the PNSC by computing a collection of references with positive and negative sequence components. It was suggested that during the voltage sag, just one of the power set-points be delivered. Through the following restrictions, this technique seeks to end power oscillations [8], [9], [35]:

$$P^* = U^+.i_p^+ + U^-.i_p^- \Rightarrow 0 = U^+.i_p^- + U^-.i_p^+ \Rightarrow i_q = 0 \tag{47}$$

$$Q^* = U_\perp^+.i_q^+ + U_\perp^-.i_q^- \Rightarrow 0 = U_\perp^+.i_q^- + U_\perp^-.i_q^+ \Rightarrow i_p = 0 \tag{48}$$

According to (47) and (48), the interactions between voltages and currents with different sequences must be removed because they cause the mean value of the instantaneous powers to arise from the products of voltages and currents with the same sequence. Therefore, the vectors of the active and reactive currents are as described in the following:

$$\mathrm{i}_\mathrm{p}^* = \frac{\mathrm{P}^*}{\left|\mathrm{U}^+\right|^2 - \left|\mathrm{U}^-\right|^2}\left(\mathrm{U}^+ - \mathrm{U}^-\right) = \mathrm{g}^\mp\left(\mathrm{U}^+ - \mathrm{U}^-\right) \tag{49}$$

$$\mathrm{i}_\mathrm{q}^* = \frac{\mathrm{Q}^*}{\left|\mathrm{U}^+\right|^2 - \left|\mathrm{U}^-\right|^2}\left(\mathrm{U}_\perp^+ - \mathrm{U}_\perp^-\right) = \mathrm{b}^\mp\left(\mathrm{U}_\perp^+ - \mathrm{U}_\perp^-\right) \tag{50}$$

in which $g\pm$ and $b\pm$, correspondingly, represent the PNSC's momentary positive/negative conductivity and verification and validation model. The goal of the PNSC is really to minimize the cosine parts of fluctuations in reactive and active powers. The sine terms are indeed still there, and the power vibrations are not zero for any of the two-power set-points that are not zero [36]. The unique point in $|\mathrm{U}+| = |\mathrm{U}-|$, or the point at which the negative and the positive sequence voltages are identical, is shown by calculations (49) and (50). This suggests that with very imbalanced voltages, it is theoretically not possible to cancel the power fluctuations [11].

$$\mathrm{i}^* = \mathrm{i}^{*+} + \mathrm{i}^{*-} \tag{51}$$

$$\mathrm{U}^+.\mathrm{i}_\mathrm{p}^{*+} + \mathrm{U}^-.\mathrm{i}_\mathrm{p}^{*-} = \mathrm{P} \tag{52}$$

$$\mathrm{U}^+.\mathrm{i}_\mathrm{p}^{*-} + \mathrm{U}^-.\mathrm{i}_\mathrm{p}^{*+} = 0 \tag{53}$$

$$\begin{aligned}\mathrm{U}^+.\mathrm{i}_\mathrm{p}^{*-} &= -\mathrm{U}^-.\mathrm{i}_\mathrm{p}^{*+} \Longrightarrow \left|\mathrm{U}^+\right|^2.\mathrm{i}_\mathrm{p}^{*-} \\ &= -\mathrm{v}^+.\mathrm{i}_\mathrm{p}^{*+}.\mathrm{U}^- \\ \Longrightarrow \mathrm{i}_\mathrm{p}^{*-} &= -\frac{\mathrm{U}^+.\mathrm{i}_\mathrm{p}^{*+}}{\left|\mathrm{U}^+\right|^2}\mathrm{U}^-\end{aligned} \tag{54}$$

$$P = \mathrm{U}^+.\mathrm{i}_\mathrm{p}^{*+}\left(1 - \frac{\left|\mathrm{U}^-\right|^2}{\left|\mathrm{U}^+\right|^2}\right) \tag{55}$$

$$\begin{aligned}&= \left|\mathrm{U}^+\right|^2.\mathrm{i}_\mathrm{p}^{*+} \Longrightarrow \mathrm{i}_\mathrm{p}^{*+} \\ &= \frac{P}{\left|\mathrm{U}^+\right|^2 - \left|\mathrm{U}^-\right|^2}\mathrm{U}^+\end{aligned} \tag{56}$$

$$U_\perp^+.\mathrm{i}_\mathrm{q}^{*+} + U_\perp^-.\mathrm{i}_\mathrm{q}^{*-} = \mathrm{Q} \tag{57}$$

$$U_\perp^+.\mathrm{i}_\mathrm{q}^{*-} + U_\perp^-.\mathrm{i}_\mathrm{q}^{*+} = 0 \tag{58}$$

$$\begin{aligned}i^* &= i_p^* + i_q^* \\ &= g^\pm\left(\mathrm{U}^+ - \mathrm{U}^-\right) + b^\pm\left(U_\perp^+ - U_\perp^-\right)\end{aligned} \tag{59}$$

$$i^+ = i_p^+ + i_q^+ \tag{60}$$

$$i^- = i_p^- + i_q^- \tag{61}$$

$$\begin{aligned}P = &\underbrace{\mathrm{U}^+ \cdot i_p^+ + \mathrm{U}^- \cdot i_p^-}_{p} + \underbrace{\mathrm{U}^+ \cdot i_q^+ + \mathrm{U}^- \cdot i_q^-}_{0} \\ &+ \underbrace{\mathrm{U}^+ \cdot i_p^- + \mathrm{U}^- \cdot i_p^+}_{0} \\ &+ \underbrace{\mathrm{U}^+ \cdot i_q^- + \mathrm{U}^- \cdot i_q^+}_{\tilde{p}}\end{aligned} \tag{62}$$

$$\begin{aligned}Q = &\underbrace{U_\perp^+ \cdot i_q^+ + U_\perp^- \cdot i_q^-}_{Q} + \underbrace{U_\perp^+ \cdot i_p^+ + U_\perp^- \cdot i_p^-}_{0} \\ &+ \underbrace{U_\perp^+ \cdot i_q^- + U_\perp^- \cdot i_q^+}_{0} \\ &+ \underbrace{U_\perp^+ \cdot i_p^- + U_\perp^- \cdot i_p^+}_{\tilde{q}}\end{aligned} \tag{63}$$

D. BALANCED POSITIVE SEQUENCE CONTROL (BPSC)

A series of completely balanced positive sequence currents with sinusoidal waveforms are produced by the BPSC. The reference currents were indeed determined with this utilizing only the positive sequence voltage vector [14], [37].

$$i_p^* = \frac{P^*}{\left|U^+\right|^2}U^+ = G^+U^+ \tag{64}$$

$$i_q^* = \frac{Q^*}{\left|U^+\right|^2} U_\perp^+ = B^+ U_\perp^+ \tag{65}$$

$$P = u.i_p^* = \underbrace{u^+ \cdot i_p^*}_{p} + \underbrace{u^- \cdot i_p^*}_{\check{p}} \tag{66}$$

$$q = u\perp.i_q^* = \underbrace{u_\perp^+ \cdot i_q^*}_{Q} + \underbrace{u_\perp^+ \cdot i_q^*}_{\check{q}} \tag{67}$$

The currents are generally approximately equal to the positive sequence voltage and the positive sequence conductivity G+ and computational neuroscience B+ are fixed. Consequently, sinusoidal currents are created by the BPSC through a positive sequence. Excluding when $P* = Q* = 0$, this methodology is unable to eliminate the power fluctuation.

IV. THE PHOTOVOLTAIC INVERTER CONTROL DESIGN

To introduce such currents into the power network, once the reference currents were precisely calculated during imbalanced voltage conditions, it also has been important to establish an appropriate current status quo. Another PI control technique on a synchronous reference frame coupled with a double synchronous reference frame has been employed in the majority of studies to date [16], [38]. Figure 2 shows a control structure with a PI controller on a stationary reference frame. The main function of MPPT is to enhance the amount of power that can be obtained from the photovoltaic system by setting the system operating voltage at the highest optimal point.

A. CONTROLLING FOR REACTIVE AND ACTIVE POWER

The following is the numerical description of both the system's reactive and active power as indirect and quadrature evolution [34], [39]:

$$\mathrm{P} = \mathrm{vd} * \mathrm{id} \tag{68}$$

$$\mathrm{q} = -\mathrm{vq} * \mathrm{iq} \tag{69}$$

Utilizing PI controllers and a feedback process, one may manage reactive and active power more precisely. Figure 3 illustrates reactive and active power feedback control.

B. SEQUENCE EXTRACTION METHOD

$$\begin{bmatrix} xd^+ \\ xq^+ \end{bmatrix} = x^+ \begin{bmatrix} \cos\left(\theta^+ - \alpha\right) \\ \sin\left(\theta^+ - \alpha\right) \end{bmatrix} + x^- \begin{bmatrix} \cos\left(-2\omega t - \theta^- - \alpha\right) \\ \sin\left(-2\omega t - \theta^- - \alpha\right) \end{bmatrix} \tag{70}$$

$$\begin{bmatrix} xd^- \\ xq^- \end{bmatrix} = x^- \begin{bmatrix} \cos\left(\theta^- - \alpha\right) \\ -\sin\left(\theta^- - \alpha\right) \end{bmatrix} + x^+ \begin{bmatrix} \cos\left(2\omega t + \theta^+ - \alpha\right) \\ \sin\left(2\omega t + \theta^+ - \alpha\right) \end{bmatrix} \tag{71}$$

where xd+, xq+, xd- and xq- are voltages or currents in positive and negative dq-frames, x+ and x- denote amplitudes of positive and negative sequences, respectively, $\theta+$ and $\theta-$ are phase shifts of positive and negative sequence components, α is the phase shift of Park transformation.

C. DC VOLTAGE CONTROLLER

The linear equation between the specified current parameter and the dc-link voltage establishes the specifications of the dc-link voltage control system. according to the photovoltaic systems system's power balance.

$$\mathrm{P_{ac}} + \mathrm{P_{dc}} + \mathrm{P_{cap}} = 0 \tag{72}$$

$$\frac{2}{3}\mathrm{vdid} + \mathrm{Vdc} * \mathrm{Idc} + \mathrm{Vdc} * \mathrm{i_{cap}} = 0 \tag{73}$$

$$\mathrm{Y\,(s)} = \frac{1}{1 + \mathrm{Ta.s}} \tag{74}$$

where Ta= T-Switch/2 Thus for the converter block,

$$\mathrm{v'_{Conv}\,(s)} \cdot \frac{1}{(1 + \mathrm{sTa})} = \mathrm{v_{Conv}\,(s)} \tag{75}$$

for which Idc and $\mathrm{i_{cap}}$ stand again for bus voltage current and capacitor current, appropriately, as well as the Park's transformation-derived 3/2 factor appears. The current flowing via the capacitor is (72).

$$\mathrm{i_{cap}} = -\left(\frac{3\mathrm{v}_d \mathrm{i}_d}{2V_{dc}} + \mathrm{I}_{dc}\right) \tag{76}$$

Additionally, the capacitor's voltage throughout the capacitor is determined according to a given current.

$$\mathrm{i_{cap}} = \mathrm{c}\frac{\mathrm{dVdc}}{\mathrm{dt}} \tag{77}$$

The mathematical expression again for dc voltage results from equations (76) and (77).

$$\frac{\mathrm{dVdc}}{\mathrm{dt}} = -\frac{3\mathrm{vdid}}{2\mathrm{c} * \mathrm{Vdc}}\left(\mathrm{id} + \frac{2\mathrm{Vdc} * \mathrm{Idc}}{3\mathrm{vd}}\right) \tag{78}$$

$$\mathrm{R\,(s)} = \mathrm{Kp} + \frac{\mathrm{Ki}}{\mathrm{s}} = \mathrm{Kp.}\left|\frac{1 + \mathrm{Ti.s}}{\mathrm{Ti.s}}\right| \tag{79}$$

$$\{\mathrm{I_{ref}\,(s)} - \mathrm{I\,(s)}\}\left(\mathrm{Kp} + \frac{\mathrm{Ki}}{\mathrm{s}}\right) = \mathrm{v_{Conv}\,(s)} \tag{80}$$

Calculation (78) indicates that such active current id influences dc link voltage. In the dc voltage controller, feedforward substitutes for something like the Idc component from formula (78). Figure 4 elsewhere here shows the schematic for dc voltage control.

D. THE OUTSIDE CONTROLLER

Real power via the converter, reactive power on either side, and dc-link voltage were also shared goals again for the outer loop. Active power flow or dc voltage range is managed

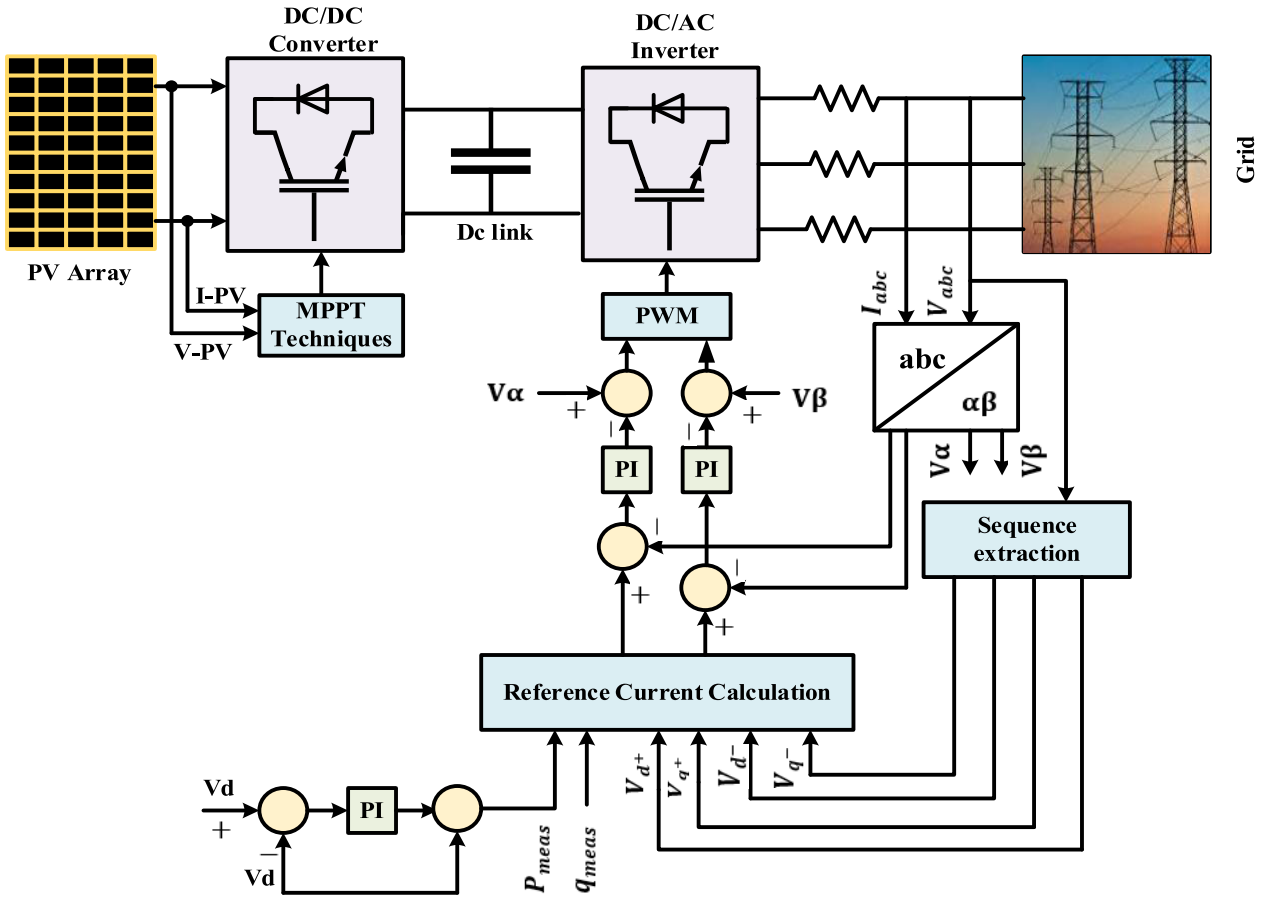

FIGURE 2. Photovoltaic inverter control system for imbalanced voltage.

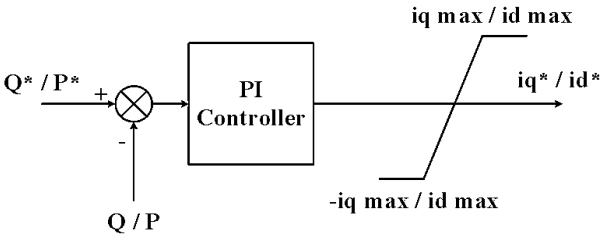

FIGURE 3. Reactive and active power monitoring schematic diagram.

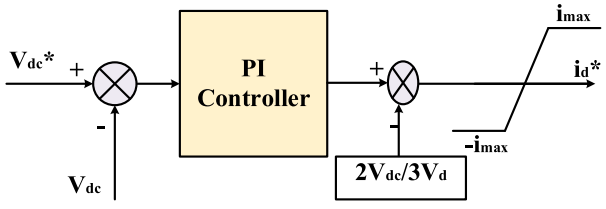

FIGURE 4. Block schematic of a dc voltage controller.

by active current (id). Related to here, reactive current (iq) is employed to regulate the flow of reactive electricity into inflexible power systems. Figure 5 represents the circuit diagram again for the outside controller [35].

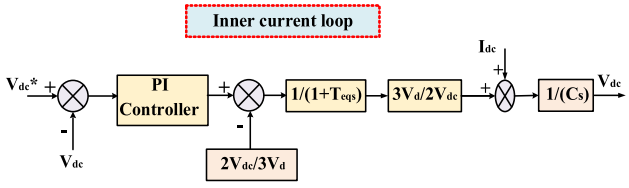

FIGURE 5. Architecture of a dc - link voltage controller's closed loop control.

V. VARIOUS TYPES OF MPPT METHODOLOGIES

We are aware that MPPT tracks the solar array since it is dependent on the temperature and solar irradiation when a PV system generates power. This section explains the four basic types of approaches that are used.

A. METHODOLOGY FOR INCREMENTAL CONDUCTANCE

A conventional photovoltaic system converts 30–40 percent of the overall ultraviolet irradiance toward electricity generated. MPP boosts the efficiency of the solar system. The power output is determined by the maximal power delivery, and it is at its highest when the impedances of the circuit and the load are matched [38]. Just using IC methodology, as illustrated in Figure 6, the operating point for the information voltage and current source is calculated. Another basis

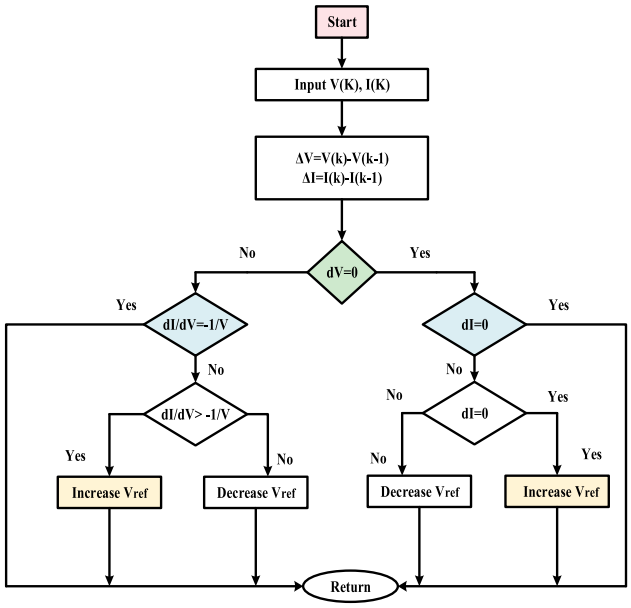

FIGURE 6. The incremental conductance algorithm's flow diagram.

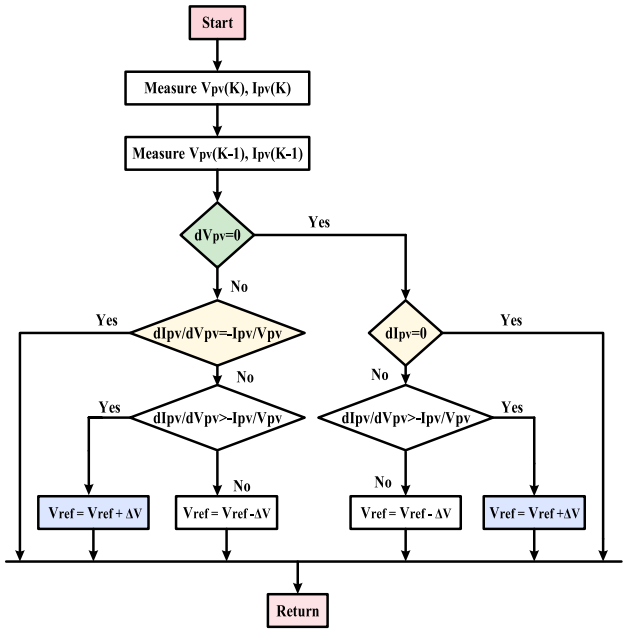

FIGURE 7. Flow chart of P & O algorithm.

for this methodology is the slope of the solar power curve concerning the voltage curve at 0 MPP. The instantaneous conductance and incremental conductance have the strongest association when [40]:

$$\frac{\Delta I}{\Delta V}+\frac{I}{V}=0 \quad \text{at MPP} \tag{81}$$

$$\frac{\Delta I}{\Delta V}+\frac{I}{V}>0 \quad \text{LEFT OF MPP} \tag{82}$$

$$\frac{\Delta I}{\Delta V}+\frac{I}{V}<0 \quad \text{RIGHT OF MPP} \tag{83}$$

With the aid of €, the MPP's amplitude is controlled. The MPP is decreasing as this rise. The measurement failure will happen as a result of system noise, and the aforementioned equation will be true. The system oscillated close to the MPP in a steady state. The $ value is deliberately selected to enhance the performance of the MPP.

B. PERTURB AND OBSERVE TECHNIQUE

The MPP is tracked using P&O. Due to the fluctuation in PV module power, this method tracks the MPP of a PV system on a mirror scale. The output power may be compared to the prior output power while measuring it, and it is periodically monitored. The same procedure is sometimes repeated when power levels rise to prevent the P&O from going backward. The power of a PV module depends on the voltage and current; as they rise or fall, so does the power [35]. To obtain the highest power outcome and to increase and minimize the PV outcome, the P&O algorithm is compelled to use the MPP as shown in Figure 7. The PV voltage increases and reduction concepts determine the direction shift of the P&O technique. During the voltage is raised, the P&O moves in the same direction, and when the voltage is dropped, the P&O moves oppositely. Additionally, this method produces the result regularly. Considering the relationship below, it is possible to determine the "D" perturbation at the time (t+ 1) [40]:

$$d\,(t+1)=d\,(t)+(2sign-1)\,D \tag{84}$$

where the sign is given by:

$$sign=([p\,(t)-p\,(t-1)]>0) \tag{85}$$

By lowering the perturbation scaling factor D, it is feasible to decrease the fluctuation from around MPP.

C. CURRENT MEASUREMENT TECHNIQUE

To measure the MPP using this approach, both voltage and current are needed. Only the PV module's current value was required for this procedure. For this technique, we connect a boost converter between the battery and, the PV panel which may store energy. The most labour-intensive aspect of this MPP is that it can get the highest possible output value from either the battery or the PV module. The principle of energy conversion makes this procedure possible [38].

$$P_{in}=V_{PV}*I_{PV} \tag{86}$$

whereas Pin symbolizes a PV array's power generated.

$$I_{out}=\frac{-(1-\delta)}{\delta}I_{PV} \tag{87}$$

$$V_{PV}\cdot I_{PV}=-V_{bat}\frac{-(1-\delta)}{\delta}I_{PV} \tag{88}$$

$$P^{*}=\frac{(1-\delta)}{\delta}I_{PV} \tag{89}$$

It often seems that the P&O method is employed when the P∗ is at its maximum since it monitors the maximum power

production from the PV system under various climatic conditions.

D. FUZZY LOGIC CONTROLLER TECHNIQUE

Based on the implementation of microprocessor circuits, everything just considers MPPT. methods because of their improved results. It relies on fuzzy logic and offers a computer for calculating power determination. When we applied the input to the MPP, a variety of errors and charges of errors appeared [37].

$$E(k) = \frac{P(k) - P(k-1)}{V(k) - V(k-1)} \tag{90}$$

$$C(E) = E(k) - E(k-1) \tag{91}$$

where P(k) and V(k) stand for the output power and voltage of a PV panel, respectively, gd D stands for defuzzification, and dD stands for the result of this. Three functional building blocks, including a fuzzy rule, an inference engine, and ultimately defuzzification, make up the fuzzy controller.

1) FUZZIFICATIONS

The previous that has been implemented according to this approach will need to use normal logic. Every other component, as well as the positive big, positive small, zero corresponding, negative medium-sized, and negative big bits, involves FLC's activity. Each technique called fuzzing has been executed twice. Initial evidence: When I define the IC methodology, E is positive whereas the MPP is flowing toward the left. The allegation of mistake is then proven. The MPP is effective when CE is negative and in the opposite mode. Second phrase: When E is negative, the MPP is on the right side; in this situation, CE will be positive and will operate on the MPP's opposite side; if E is negative, it will work on the MPP's opposite side.

2) DEFUZZIFICATION

The FLC's crisp output was estimated throughout this operation. It describes the fuzzy logic statement space.

Corresponding to the MPP at different temperatures and irradiance. As the irradiance increases at a constant temperature, the voltage, and current increase and, consequently, the PV-generated power as shown in Figures 8(a) and 8(b). While if the temperature increases at constant irradiance, the PV voltage is almost constant, and the current decreases. Consequently, the PV-generated power decreases, as depicted in the PV-generated power is affected mainly by the values of the irradiances and temperatures. In addition, the DC output voltage of the DC-DC converter significantly affects the power extracted from the PV system hence controlling this DC voltage to the value at which MPP is used to achieve MPPT.

VI. SIMULATION RESULTS

This study aims to propose a photovoltaic system model by using SIMULINK / MATLAB tools to examine if the proposed method of control seems to be adequate. Figure 3 demonstrates the Photovoltaic inverter, which also uses the dual current modulation technique and the structure diagrams. Table 1 is a summary of the PV system input parameters.

Initially, we based our calculations on a standard 3-phase system with a 0.5-s phase voltage drip and assumed the fault type is permanent and not transient. Power drops from 100 kW to 80 kW without regulation are depicted on the response curve of reactive and active power in Figure 9.

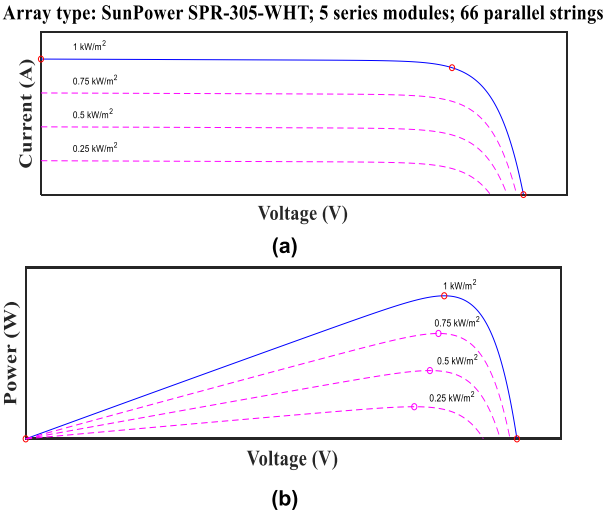

FIGURE 8. PV system characteristics at irradiation change (a) I-V characteristics, (b) P-V characteristics.

TABLE 1. Designed to simulate PV Inverter Implementation of sustainable.

Parameters	Value
Real Power normal / kW	100
DC Voltage / V	500
DC Capacitor / F	0.0006
Grid Inductance / H	0.0017
Sampling Frequency / HZ	8000

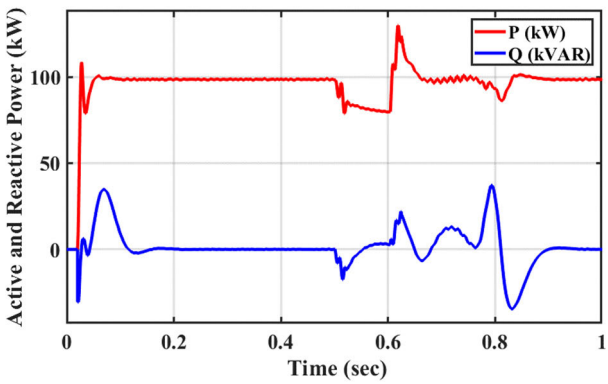

FIGURE 9. The system's both active and reactive power.

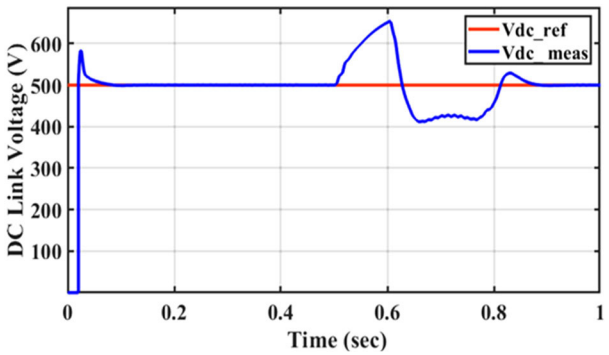

FIGURE 10. The system's dc link voltage.

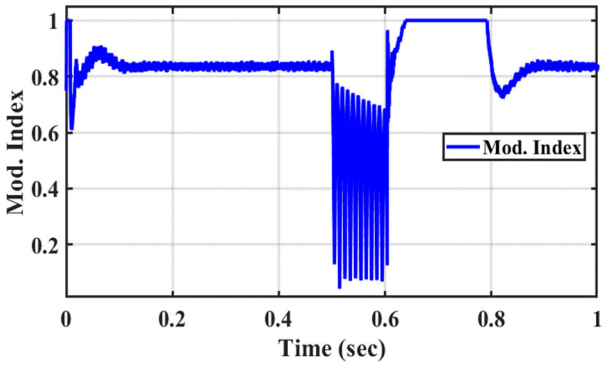

FIGURE 11. The VSC's modulation index.

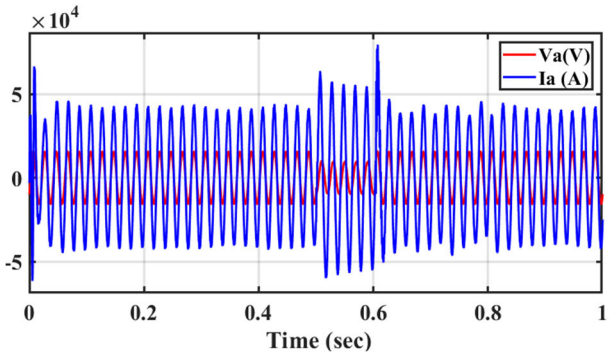

FIGURE 12. The grid's phase voltage and current.

In Figure 10, we see how large variations in the response curve of DC link voltage occur in response to voltage dips where the voltage has risen to 700 V and dropped to 400 V through the time duration voltage dip. The curve of the VSC modulation index is presented in Figure 11 the modulation index drops from 0.85 to 0.15 as the voltage drops After the specified failure period, the fault is removed and the system returns to its first position, and this indicates the effectiveness of the control system. The voltage and current of a grid phase during a fault are shown in Figure 12.

The network current's behaviours toward the IARC approach are displayed in Figure 13(a). One of the flaws in this control method is demonstrated by the figure, which

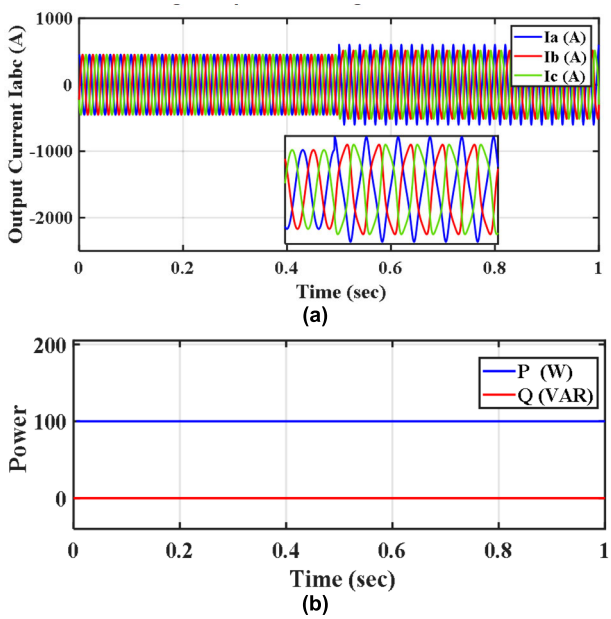

FIGURE 13. Employing the IARC approach, grid currents, and real and reactive power. (a) Grid currents using IARC method, (b) IARC-based reactive and active powers.

demonstrates how network currents are out of balance during fault time. Figure 13(b), but at the other hand, displays the response of both active and reactive power using the same methodology, but in this case, the stability of the active and reactive power remains constant, regardless of the event of failure, which is a benefit of this methodology. Figure 14(a) illustrates the DC voltage, which exhibits a significant amount of variation. Also, Figure 14(b) displays the network voltage when the IARC approach is being used, demonstrating how the voltage dip emerges all across the fault's specified period.

Figure 17 demonstrates the network currents as well as their active and reactive powers when using the BPSC method. Figure 17 (a) displays how the BPSC approach is applied to represent the grid current. The figure suggests that the currents remain in a condition of equilibrium throughout the voltage drop, which lasts between 0.5 and 1 second. and here it is assumed that the type of fault is permanent until the effect of control appears on the system.

Figure 17(b), on the other hand, depicts the temporal response of each active and reactive power when employing the same technology. This figure has huge, fixed harmonic, and disturbances placed on it, which would be detrimental to the system's overall stability. The reaction to both the network voltage and the DC link voltage is also seen in Fig. 18. Figure 18(a) shows the network voltage measured with the BPSC method during the voltage dip that occurred between 0.5 and 1. On the other hand, Figure 18(b) indicates the temporal response to the DC link voltage when employing the same approach, demonstrating the positive effects of active control and a stable system. The application of the PNSC

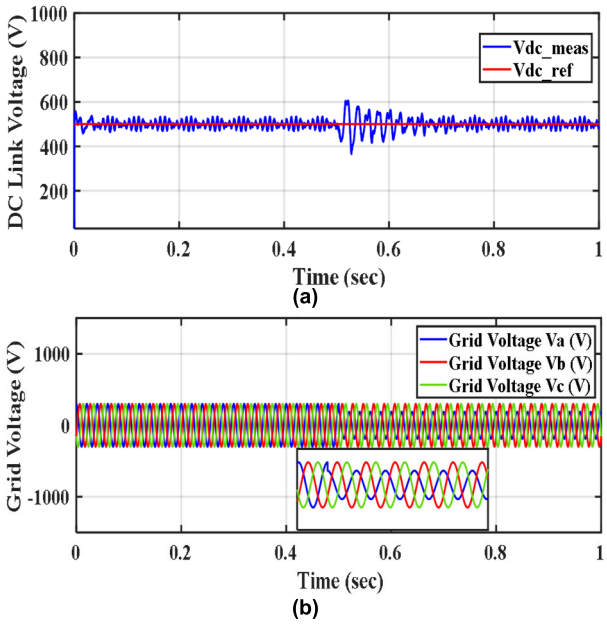

FIGURE 14. Grid voltage, and dc link voltage using IARC control. (a) dc link voltage using IARC method, (b) Grid voltage using IARC method.

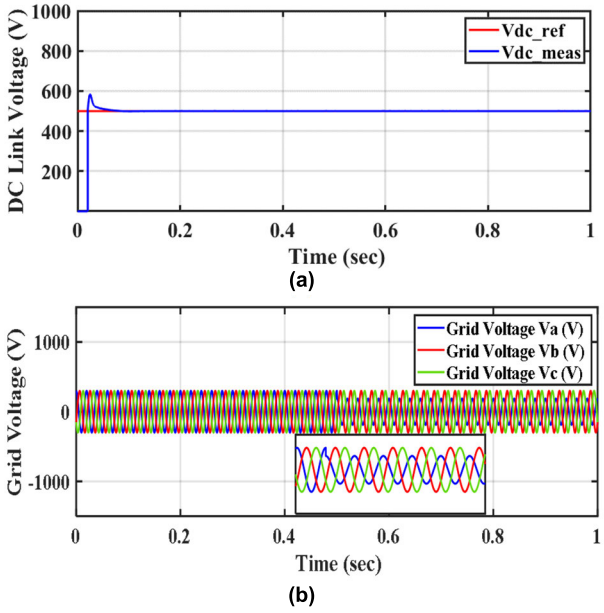

FIGURE 16. Grid voltage, and dc link voltage using PNSC control (a) dc link voltage using PNSC method, (b) Grid voltage using PNSC method.

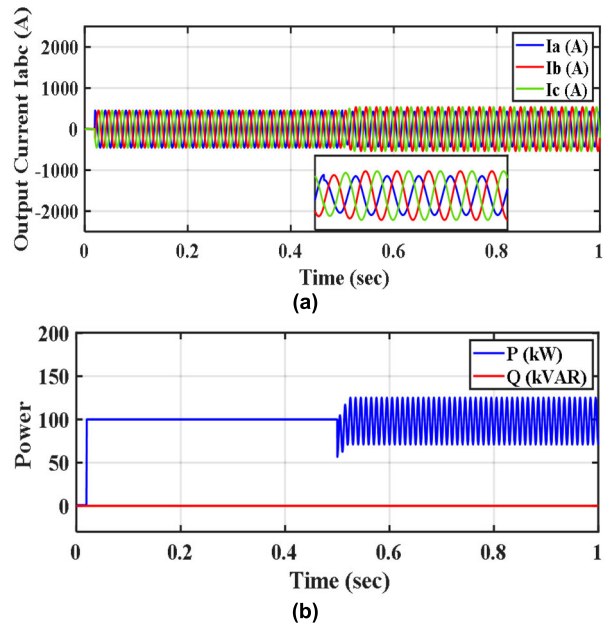

FIGURE 15. PNSC control of grid currents, active power, and reactive power. (a) Grid currents using PNSC method, (b) PNSC technique for both reactive and active powers.

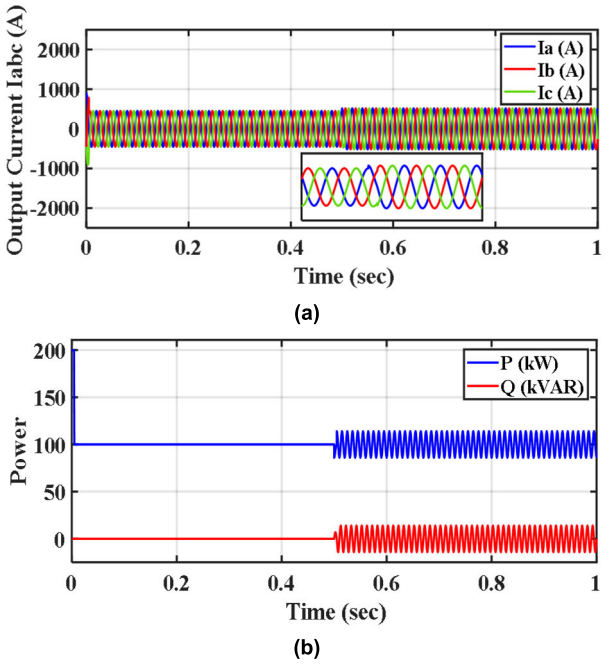

FIGURE 17. BPSC regulation of grid currents, active power, and reactive power. (a) Grid currents using BPSC method, (b) BPSC technique for both active and reactive powers.

control strategy reveals that the active power oscillates in the case of a failure regardless of the constant reactive power as shown in Figure 15(b) and that the currents sent into the grid are balanced and low-harmonic polluted, as shown in Figure 15(a). For the AARC methodology, the active power, reference is maintained at a constant at its reference P∗g, although the reactive power reference is kept at zero. The injected currents are predicted to be sinusoidal and out of balance in amplitude when an imbalance develops, as shown by Figures 19(a), 19(b), 20(a), and 20(b). The voltages at the point of common connection are followed by these currents. On the other hand, the active power exhibits oscillations at double the fundamental frequency. Further, Table 2 references current calculation methodologies that can eliminate oscillations in reactive power for those who have used this

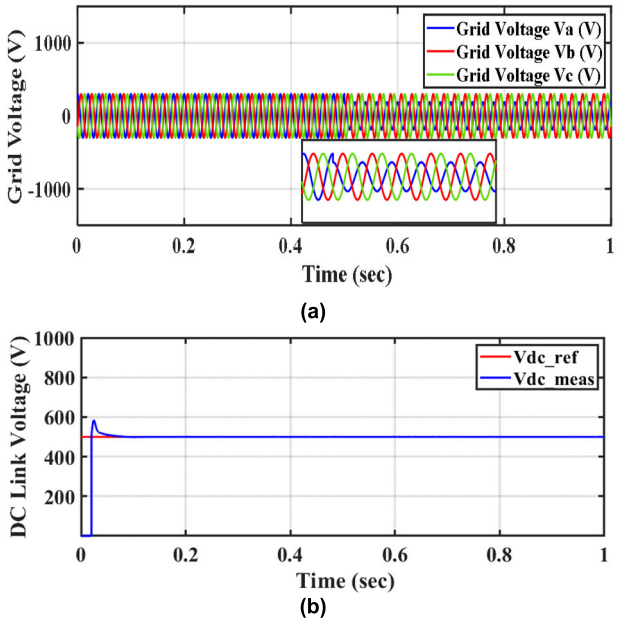

FIGURE 18. Grid voltage, and dc link voltage using BPSC control (a) Grid voltage using BPSC method, (b) dc link voltage using BPSC method.

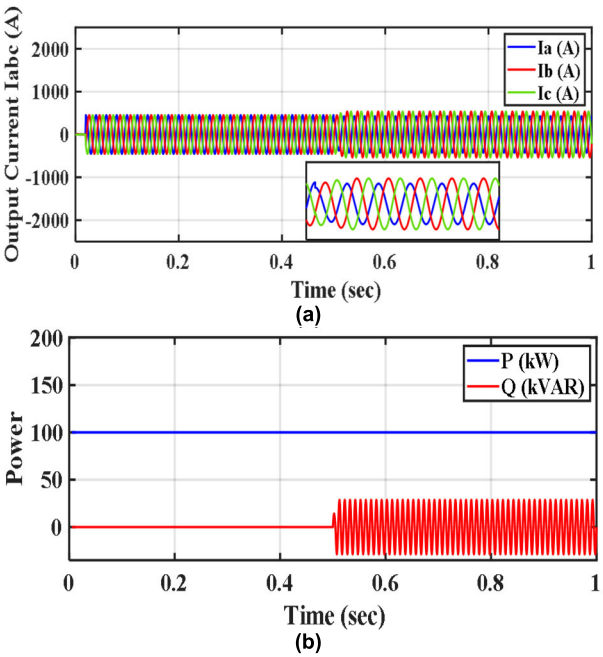

FIGURE 19. AARC management of grid currents, reactive power, and active power. (a) Grid currents using AARC method, (b) AARC methodology for both reactive and active powers.

methodology. Figure 23 illustrates the performance parameters of the monitored power produced from the four MPPT controllers under standard settings. The FLC is believed to attain MPP more quickly compared to the other controllers. The FLC method will produce a better-constructed performance for the PV system (Figure 23) compared with the other MPPT techniques. Consequently, there has been a huge reduction in power consumption.

The effectiveness of the PV system that utilizes the four MPPT ways can be seen in Figure 22 during conditions of constant irradiation and temperature, whereas FLC, Current Only, and INC approaches seemed to have constant dc link voltage although the P&O method indicates excessive fluctuation. Figures 22 and 23 depict the four controllers' effectiveness within conditions of constant temperature and irradiance. The simulation findings indicate that the four controllers' performances are relatively comparable under varying meteorological circumstances. The values of power and dc-link voltage for 4 distinct MPPT techniques are shown in Table 3 at constant temperature and irradiation. Figure 21, on the other hand, depicts the system under the study of each positive and negative sequence component when employing the different techniques to control active and reactive power in a grid-connected PV system.

In a power system, the balance between power generation and consumption is critical for ensuring the stability and reliability of the grid. However, under certain circumstances, such as the integration of large amounts of renewable energy sources, the power system may become unbalanced, leading to a range of technical challenges. This is particularly relevant for photovoltaic (PV) systems, which are increasingly being deployed in the electricity grid. During voltage imbalance,

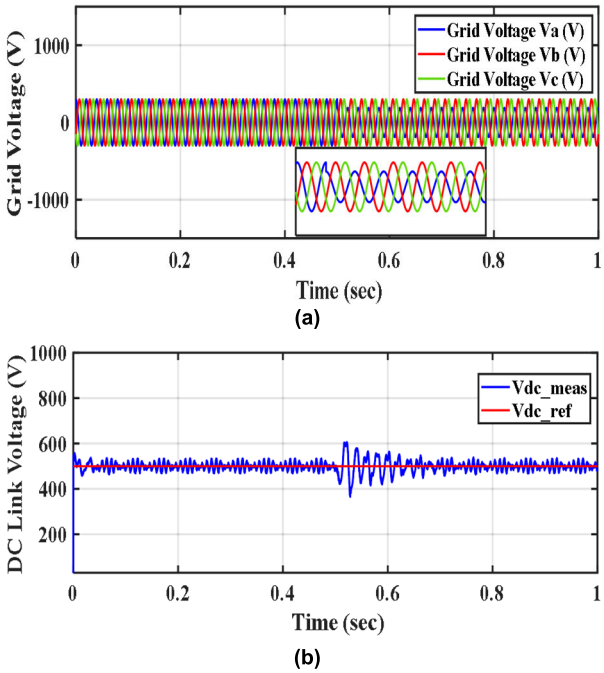

FIGURE 20. Grid voltage, and dc link voltage using AARC control (a) Grid voltage using AARC method, (b) dc link voltage using AARC method.

the current increases while the voltage decreases, resulting in an increase in the duty cycle value from 0.45 to 0.78. Additionally, the DC link voltage fluctuates between 400 and 750 volts, causing an increase in power. Based on these observations, the value of the reference current and voltage

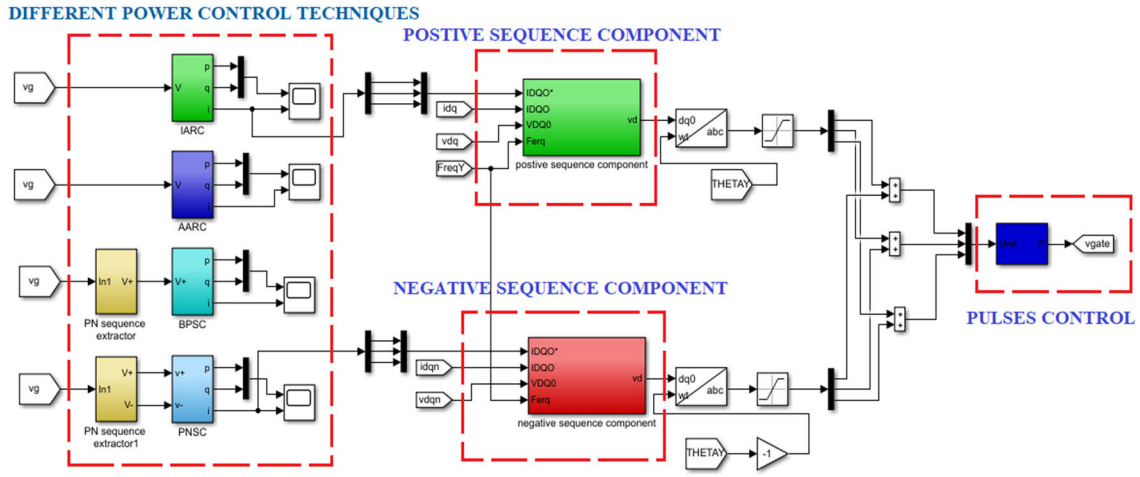

FIGURE 21. The control power system under study.

TABLE 2. Features of the reference current calculation strategies.

strategy	$p \neq 0; \breve{p} = 0$ $Q^* = 0\ Q^* \neq 0$		$Q \neq 0; \breve{q} = 0$ $p^* = 0\ p^* \neq 0$		$p \neq 0; \breve{q} = 0$ $Q^* = 0\ Q^* \neq 0$		$Q \neq 0; \breve{p} = 0$ $P^* = 0\ P^* \neq 0$		I_{harm}	Equipment
IARC	×	×	×	×	×	×	×	×	×	simple
PNSC	×	√	×	√	×	√	√	√	√	Acceptable
AARC	√	√	√	√	√	×	×	√	√	fairly simple
BPSC	√	√	√	√	√	√	×	√	√	complex

TABLE 3. Comparison of output power for different techniques at constant temperature and irradiation.

Irradiation (W/m^2)	Temperature (^{0}C)	Methods		Power (Kw)		DC Link Voltage (V)	
1000	25		Fuzzy Logic		100		500
			Current only		99.45		498
			INC		96.03		496
			P & O		94.26		494.45

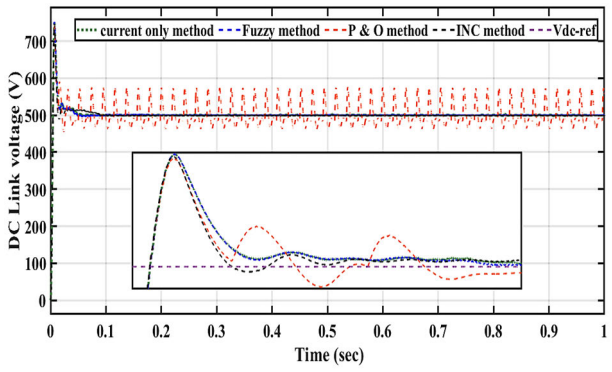

FIGURE 22. DC link voltage with different methods for MPPT.

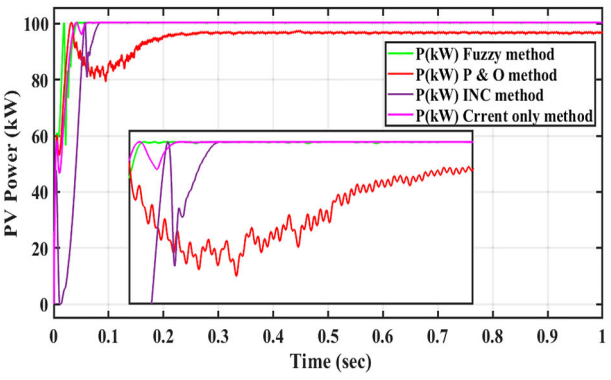

FIGURE 23. Time response of PV source power with different methods for MPPT.

is calculated and found to be approximately 1.2 p-u as shown in Fig. 24.

In particular, unbalanced grid conditions can result in the following impacts on the PV system: Reduced energy yield: When the grid voltage deviates from its nominal value, the power output of the PV system is affected. If the voltage is too high, the PV system may reduce its output to avoid

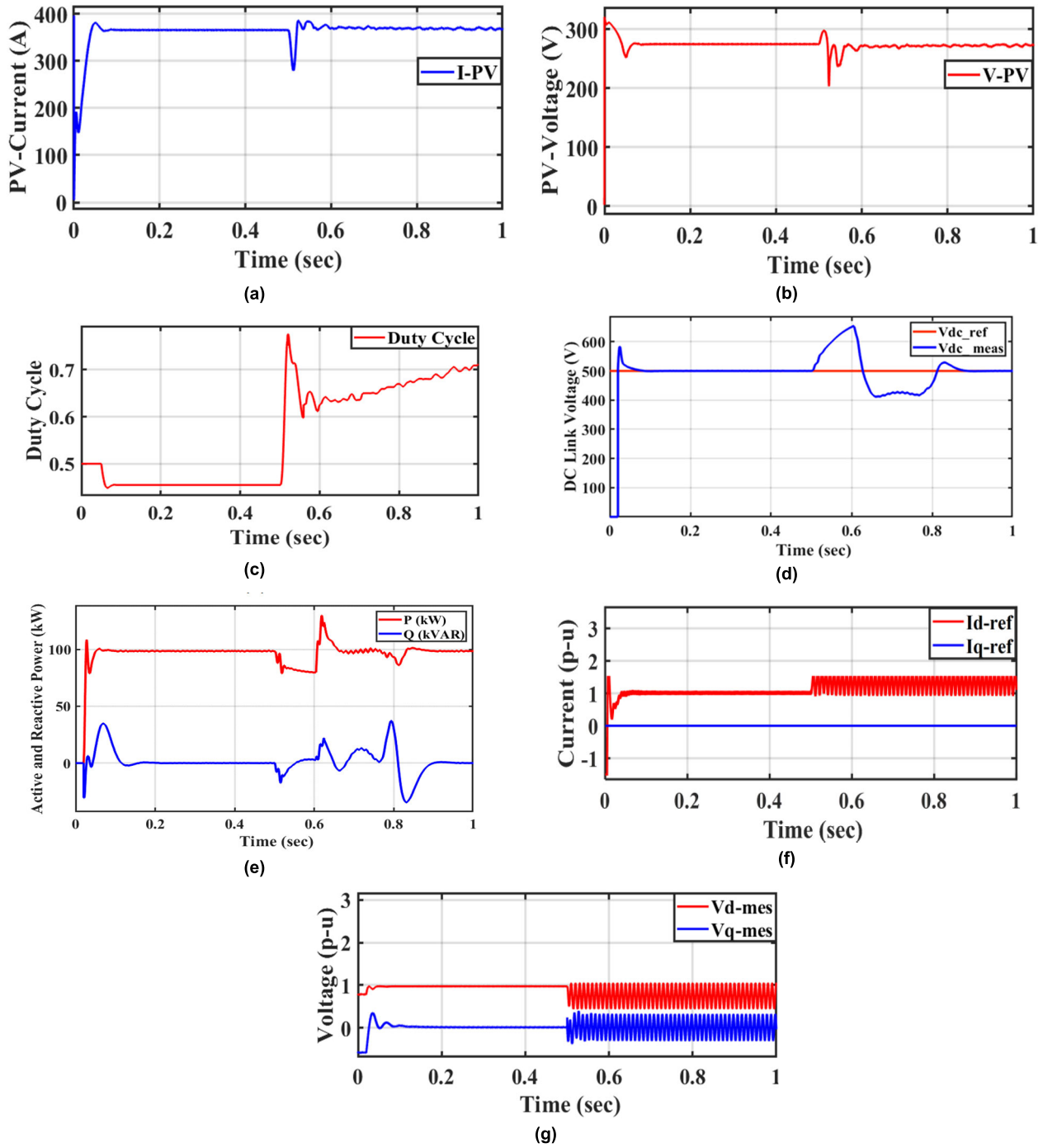

FIGURE 24. Impact of the unbalanced grid conditions on the PV system (a) PV-Current, (b) PV-Voltage, (c) Duty cycle, (d) dc link voltage, (e) active and reactive power, (f) current reference, and (g) voltage reference.

overvoltage conditions, whereas if the voltage is too low, the PV system may not be able to inject power into the grid. This can result in a reduced energy yield from the PV system. Increased stress on the inverter: The inverter is a critical component of the PV system that converts DC power from the PV panels into AC power that can be injected into the grid. Under unbalanced grid conditions, the inverter may need to operate outside its normal operating range, which can increase stress on the inverter and reduce its lifespan. Unstable operation: Unbalanced grid conditions can cause instability in the PV system, which can result in voltage and frequency fluctuations that can damage the PV system and other components in the grid.

Safety risks: Under unbalanced grid conditions, the PV system may not be able to disconnect from the grid in a timely and safe manner, which can pose a safety risk to both

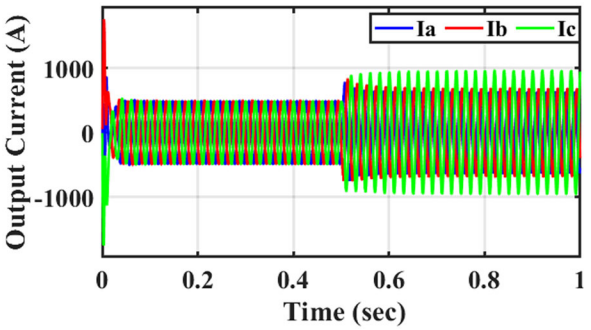

FIGURE 25. Impact of the unbalanced grid conditions on the overcurrent.

the system and the personnel working on it. To mitigate the impact of unbalanced grid conditions on PV systems, various measures can be implemented, including voltage regulation, active power control, and reactive power control. These measures can help to maintain the stability and reliability of the grid and ensure that the PV system operates safely and efficiently.

Figure 25 represents the current waveform during unbalanced grid conditions at 0.5 s to 1 s. It is found that the current increased from 500 A to approximately 1000 A, this is the illiterate impact of unbalanced grid conditions on overcurrent.

VII. CONCLUSION

In this study, four methodological approaches are proposed and evaluated for controlling unbalanced photovoltaic systems that are connected to the network. The primary areas of concentration are creating different balanced positive AC currents or forming the current references responsible for controlling the offered reactive and active power fluctuations. The results indicate that selecting the most effective method for managing a particular reactive power sometimes requires accepting a few additional sacrifices. However, it is important to evaluate the predetermined criteria to understand how the scheme is reliant on the demands of the utility network.

After presenting four different approaches for controlling photovoltaic systems connected to the network under unbalanced conditions, it was found that the BPSC method is the most effective with a success rate of 90%. This is because it ensures balanced currents and minimal fluctuations in active and reactive power, which do not exceed 0.1 of the total power. Additionally, the DC voltage value is fixed at 500 volts, which is comparable to other methods. However, the only downside of the BPSC method is its complex construction when compared to other methods. The study compares four control methods that can greatly minimize output harmonics and fluctuations in both reactive and active power. The FLC approach is quicker than other MPPT approaches (P&O and IC) since it provides a better outcome for getting statistics.

The FL method was implemented to improve the effective power output of the system, resulting in an increase to 100 kW. The maximum overshoot % is 0.5612, while the rise time is 0.0325 s, and the setting time is equal to 3.6752 s. Furthermore, the FL method was utilized to enhance the dc link voltage of the system, which was found to be equal to 500 V. The maximum overshoot % for the voltage is 0.42, while the rise time is 0.0038 s, and the setting time is 0.0391 s. Although the rising current generation entails large power fluctuations, minimizing power system oscillations yields deformed currents. Thus, it is evidenced that MPPT is necessary for enhancing the quality of such a PV panel arrangement. In future work, the experimental application of the proposed method will be studied in a grid-connected PV system.

REFERENCES

[1] G. Son and Q. Li, "Control techniques for CRM-based high-frequency soft-switching three-phase inverter under unbalanced grid conditions," *IEEE Trans. Power Electron.*, vol. 37, no. 6, pp. 6613–6624, Jun. 2022.

[2] H. Abubakr, J. C. Vasquez, K. Mahmoud, M. M. F. Darwish, and J. M. Guerrero, "Comprehensive review on renewable energy sources in egypt—Current status, grid codes and future vision," *IEEE Access*, vol. 10, pp. 4081–4101, 2022.

[3] F. Wu, R. Liu, Y. Xie, and J. Lyu, "A modified power decoupling control strategy for a grid-connected inverter with a low switching frequency under unbalanced grid voltages," *Energy Rep.*, vol. 8, pp. 757–768, Aug. 2022.

[4] P. Cheng, K. Li, C. Wu, J. Ma, and L. Jia, "Flexible power regulation and limitation of voltage source inverters under unbalanced grid faults," *CES Trans. Electr. Mach. Syst.*, vol. 6, no. 2, pp. 153–161, Jun. 2022.

[5] P. P. Vergara, M. Salazar, J. S. Giraldo, and P. Palensky, "Optimal dispatch of PV inverters in unbalanced distribution systems using reinforcement learning," *Int. J. Electr. Power Energy Syst.*, vol. 136, Mar. 2022, Art. no. 107628.

[6] K. Gholami, S. Karimi, and A. Anvari-Moghaddam, "Multi-objective stochastic planning of electric vehicle charging stations in unbalanced distribution networks supported by smart photovoltaic inverters," *Sustain. Cities Soc.*, vol. 84, Sep. 2022, Art. no. 104029.

[7] V. R. Chowdhury, M. M. Biswas, and D. Chowdhury, "Lyapunov energy function based control of a PV based current source inverter under unbalanced grid voltage condition," in *Proc. 47th Annu. Conf. IEEE Ind. Electron. Soc.*, Oct. 2021, pp. 1–6.

[8] C.-Y. Tang and C.-J. Cheng, "DC-link voltage ripple cancellation strategies for three-phase four-wire PV inverters under unbalanced grid voltages," in *Proc. IEEE Int. Future Energy Electron. Conf. (IFEEC)*, Nov. 2021, pp. 1–6.

[9] S. Yazdani, M. Ferdowsi, M. Davari, and P. Shamsi, "Advanced current-limiting and power-sharing control in a PV-based grid-forming inverter under unbalanced grid conditions," *IEEE J. Emerg. Sel. Topics Power Electron.*, vol. 8, no. 2, pp. 1084–1096, Jun. 2020.

[10] M. Wang, X. Zhang, T. Zhao, F. Zhuang, F. Wang, N. Qian, and S. Yang, "Module power balance control strategy for three-phase cascaded H-bridge PV inverter under unbalanced grid voltage condition," *IEEE J. Emerg. Sel. Topics Power Electron.*, vol. 9, no. 5, pp. 5657–5671, Oct. 2021.

[11] L. H. Lam, T. D. H. Phuc, and N. H. Hieu, "Simulation models for three-phase grid connected PV inverters enabling current limitation under unbalanced faults," *Eng., Technol. Appl. Sci. Res.*, vol. 10, no. 2, pp. 5396–5401, Apr. 2020.

[12] O. Husev, N. V. Kurdkandi, M. G. Marangalu, D. Vinnikov, and S. H. Hosseini, "A new single-phase flying inductor-based common grounded converter for dual-purpose application," *IEEE Trans. Ind. Electron.*, vol. 70, no. 8, pp. 7913–7923, Aug. 2023.

[13] N. V. Kurdkandi, M. G. Marangalu, O. Husev, A. Aghaie, M. R. Islam, Y. P. Siwakoti, K. M. Muttaqi, and S. H. Hosseini, "A new seven-level transformer-less grid-tied inverter with leakage current limitation and voltage boosting feature," *IEEE J. Emerg. Sel. Topics Ind. Electron.*, vol. 4, no. 1, pp. 228–241, Jan. 2023.

[14] S. Abbasi, A. A. Ghadimi, A. H. Abolmasoumi, M. Reza Miveh, and F. Jurado, "Enhanced control scheme for a three-phase grid-connected PV inverter under unbalanced fault conditions," *Electronics*, vol. 9, no. 8, p. 1247, Aug. 2020.

[15] N. F. Ibrahim, M. Fawzi, H. A. Ibrahim, and S. S. Dessouky, "Control strategies for VSC based HVDC during grid faults: A comparative study of selection criteria of currents reference," in *Proc. 21st Int. Middle East Power Syst. Conf. (MEPCON)*, Dec. 2019, pp. 311–315.

[16] N. F. Ibrahim, S. S. Dessouky, H. E. M. Attia, and A. H. K. Alaboudy, *Protection of Wind Turbine Generators Using Microcontroller-Based Applications*. Berlin, Germany: Springer, 2022.

[17] A. Q. Al-Shetwi, M. A. Hannan, K. P. Jern, A. A. Alkahtani, and A. E. P. Abas, "Power quality assessment of grid-connected PV system in compliance with the recent integration requirements," *Electronics*, vol. 9, no. 2, p. 366, Feb. 2020.

[18] N. Babu P, J. M. Guerrero, P. Siano, R. Peesapati, and G. Panda, "An improved adaptive control strategy in grid-tied PV system with active power filter for power quality enhancement," *IEEE Syst. J.*, vol. 15, no. 2, pp. 2859–2870, Jun. 2021.

[19] A. Elkholy, "Harmonics assessment and mathematical modeling of power quality parameters for low voltage grid connected photovoltaic systems," *Sol. Energy*, vol. 183, pp. 315–326, May 2019.

[20] S. Zhou, Y. Han, S. Chen, P. Yang, K. Mahmoud, M. M. F. Darwish, L. Matti, and A. S. Zalhaf, "A multiple uncertainty-based bi-level expansion planning paradigm for distribution networks complying with energy storage system functionalities," *Energy*, vol. 275, Jul. 2023, Art. no. 127511.

[21] P. Shukl and B. Singh, "Recursive digital filter based control for power quality improvement of grid tied solar PV system," *IEEE Trans. Ind. Appl.*, vol. 56, no. 4, pp. 3412–3421, 2020.

[22] A. Gupta, "Power quality evaluation of photovoltaic grid interfaced cascaded H-bridge nine-level multilevel inverter systems using D-STATCOM and UPQC," *Energy*, vol. 238, Jan. 2022, Art. no. 121707.

[23] F. K. Abo-Elyousr, A. M. Sharaf, M. M. F. Darwish, M. Lehtonen, and K. Mahmoud, "Optimal scheduling of DG and EV parking lots simultaneously with demand response based on self-adjusted PSO and K-means clustering," *Energy Sci. Eng.*, vol. 10, no. 10, pp. 4025–4043, Oct. 2022.

[24] Y. Liu, M. Wang, Z. Xu, and S. Yan, "MPC control of three-phase CSI in unbalanced grid," in *Proc. Int. Conf. Power Energy Syst. Appl. (ICoPESA)*, Feb. 2022, pp. 357–361.

[25] Prashant, M. Sarwar, A. S. Siddiqui, S. S. M. Ghoneim, K. Mahmoud, and M. M. F. Darwish, "Effective transmission congestion management via optimal DG capacity using hybrid swarm optimization for contemporary power system operations," *IEEE Access*, vol. 10, pp. 71091–71106, 2022.

[26] A. Bouhouta, S. Moulahoum, and N. Kabache, "A novel combined fuzzy-M5P model tree control applied to grid-tied PV system with power quality consideration," *Energy Sources, A, Recovery, Utilization, Environ. Effects*, vol. 44, no. 2, pp. 3125–3147, Jun. 2022.

[27] M. A. Mohamed, A. Y. Abdelaziz, M. M. F. Darwish, M. Lehtonen, and K. Mahmoud, "Optimum estimation of series capacitors for enhancing distribution system performance via an improved hybrid optimization algorithm," *Energy Sci. Eng.*, pp. 1–19, Feb. 2023, doi: 10.1002/ese3.1426.

[28] D. Çelik and M. E. Meral, "A flexible control strategy with overcurrent limitation in distributed generation systems," *Int. J. Electr. Power Energy Syst.*, vol. 104, pp. 456–471, Jan. 2019.

[29] D. Çelik and M. E. Meral, "A novel control strategy for grid connected distributed generation system to maximize power delivery capability," *Energy*, vol. 186, Nov. 2019, Art. no. 115850.

[30] Y. Zhang and Z. Min, "Model-free predictive current control of a PWM rectifier based on space vector modulation under unbalanced and distorted grid conditions," *IEEE J. Emerg. Sel. Topics Power Electron.*, vol. 10, no. 2, pp. 2319–2329, Apr. 2022.

[31] P. Zhang, X. Wu, S. He, W. Xu, J. Liu, J. Qi, and A. Yang, "A second-order voltage ripple suppression strategy of five-level flying capacitor rectifiers under unbalanced AC voltages," *IEEE Trans. Ind. Electron.*, vol. 70, no. 2, pp. 1140–1149, Feb. 2023.

[32] M. Cheng, X. Yan, and J. Zhou, "Negative-sequence current compensation-based coordinated control strategy for dual-cage-rotor brushless doubly fed induction generator under unbalanced grid conditions," *IEEE Trans. Ind. Electron.*, vol. 70, no. 5, pp. 4762–4773, May 2023.

[33] A. A. Elbaset, S. A. M. Abdelwahab, H. A. Ibrahim, and M. A. E. Eid, *Performance Analysis of Photovoltaic Systems With Energy Storage Systems*. Berlin, Germany: Springer, 2019.

[34] H. Hao, X. Yonghai, and Y. Lin, "Control scheme of PV inverter under unbalanced grid voltage," in *Proc. IEEE PES Gen. Meeting Conf. Expo.*, Jul. 2014, pp. 1–5.

[35] N. F. Ibrahim and S. S. Dessouky, *Design and Implementation of Voltage Source Converters in HVDC Systems*. Berlin, Germany: Springer, 2021.

[36] M. N. Ali, M. Soliman, K. Mahmoud, J. M. Guerrero, M. Lehtonen, and M. M. F. Darwish, "Resilient design of robust multi-objectives PID controllers for automatic voltage regulators: D-decomposition approach," *IEEE Access*, vol. 9, pp. 106589–106605, 2021.

[37] M. N. Ali, K. Mahmoud, M. Lehtonen, and M. M. F. Darwish, "Promising MPPT methods combining metaheuristic, fuzzy-logic and ANN techniques for grid-connected photovoltaic," *Sensors*, vol. 21, no. 4, p. 1244, Feb. 2021.

[38] H. Abubakr, J. M. Guerrero, J. C. Vasquez, T. H. Mohamed, K. Mahmoud, M. M. F. Darwish, and Y. A. Dahab, "Adaptive LFC incorporating modified virtual rotor to regulate frequency and tie-line power flow in multi-area microgrids," *IEEE Access*, vol. 10, pp. 33248–33268, 2022.

[39] S. Zhou, Y. Han, P. Yang, K. Mahmoud, M. Lehtonen, M. M. F. Darwish, and A. S. Zalhaf, "An optimal network constraint-based joint expansion planning model for modern distribution networks with multi-types intermittent RERs," *Renew. Energy*, vol. 194, pp. 137–151, Jul. 2022.

[40] M. A. E. Eid, A. A. Elbaset, H. A. Ibrahim, and S. A. M. Abdelwahab, "Modelling, simulation of MPPT using perturb and observe and incremental conductance techniques for stand-alone PV systems," in *Proc. 21st Int. Middle East Power Syst. Conf. (MEPCON)*, Dec. 2019, pp. 429–434.

NAGWA F. IBRAHIM received the B.Sc. degree from the Faculty of Industrial Education, Suez Canal University, Suez, Egypt, in 2008, and the M.Sc. and Ph.D. degrees from the Faculty of Industrial Education, Suez University, Suez, in 2015 and 2019, respectively. She is currently an Assistant Professor with the Department of Electrical Power and Machine, Faculty of Technology and Education, Suez University. Her research interests include renewable energy sources, power system protection, power electronics, high-voltage direct current (HVDC), control and power quality issues, and the control of power electronic converters and electrical machine drives.

KARAR MAHMOUD (Senior Member, IEEE) received the B.Sc. and M.Sc. degrees in electrical engineering from Aswan University, Aswan, Egypt, in 2008 and 2012, respectively, and the Ph.D. degree from the Electric Power and Energy System Laboratory (EPESL), Graduate School of Engineering, Hiroshima University, Hiroshima, Japan, in 2016. Since 2010, he has been with Aswan University, where he is currently an Associate Professor with the Department of Electrical Engineering, Faculty of Engineering. He is also a Postdoctoral Researcher with the Group of Prof. M. Lehtonen, School of Electrical Engineering, Aalto University, Finland. He has authored or coauthored several publications in top-ranked journals, including IEEE journals, international conferences, and book chapters. His research interests include power systems, renewable energies, smart grids, distributed generation, optimization, applied machine learning, the IoT, industry 4.0, and high-voltage. Since 2021, he has been a Topic Editor of *Sensors* journal (MDPI). He is an Associate Editor of the journals *IET Generation, Transmission and Distribution* and *Frontiers in Energy Research*.

MATTI LEHTONEN received the master's and Licentiate degrees in electrical engineering from the Helsinki University of Technology, Finland, in 1984 and 1989, respectively, and the Doctor of Technology degree from the Tampere University of Technology, Finland, in 1992. He was with VTT Energy, Espoo, Finland, from 1987 to 2003. Since 1999, he has been a Full Professor and the Head of the Power Systems and High Voltage Engineering Group, Aalto University, Espoo. His research interests include power system planning and assets management and power system protection, including earth fault problems, harmonic related issues, high-voltage systems, power cable insulation, and polymer nanocomposites. He is an Editor of *IET Generation, Transmission and Distribution* journal and an Associate Editor of the *Electric Power Systems Research* journal.

MOHAMED M. F. DARWISH (Senior Member, IEEE) was born in Cairo, Egypt. He received the B.Sc., M.Sc., and Ph.D. degrees in electrical engineering from the Faculty of Engineering at Shoubra, Benha University, Cairo, in May 2011, June 2014, and January 2018, respectively.

From 2016 to 2017, he joined as a Ph.D. Student with the Department of Electrical Engineering and Automation (EEA), Aalto University, Finland, and the Prof. M. Lehtonen's Group. He is currently an Associate Professor with the Department of Electrical Engineering, Faculty of Engineering at Shoubra, Benha University. He is also a Postdoctoral Researcher with the Department of EEA, School of Electrical Engineering, Aalto University. He has authored several international IEEE journals and conferences. His research interests include HV polymer nanocomposites, nano-fluids, fault diagnosis, renewables, optimization, applied machine learning, the IoT, industry 4.0, and control systems. He received the Best Ph.D. Thesis Prize that serves industrial life and society all over the Benha University Staff for the academic year (2018–2019). He also received the Benha University Encouragement Award in the field of engineering sciences for the academic year (2021–2022). Since 2021, he has been a Topic Editor of *Catalysts* journal (MDPI) and a guest editor of several special issues. In 2022, he has been nominated as a Young Editorial Board Member of *Applied Energy* journal. He was an Associate Editor of *IET Generation, Transmission and Distribution* journal, *Electric Power Components and Systems* journal, and *Frontiers in Energy Research* journal.